Water Research 248 (2024) 120844

Contents lists available at ScienceDirect

Water Research

journal homepage: www.elsevier.com/locate/watres

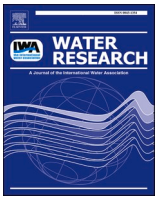

Impact of iron addition on phosphorus dynamics in sediments of a shallow peat lake 10 years after treatment

Melanie A. Münch [a,*], Rianne van Kaam [a], Karel As [b], Stefan Peiffer [b], Gerard ter Heerdt [c], Caroline P. Slomp [a,d], Thilo Behrends [a]

[a] Utrecht University, Princetonlaan 8A, 3584CB Utrecht, the Netherlands
[b] University of Bayreuth, Universitätsstrasse 30, 95440 Bayreuth, Germany
[c] Waternet, Korte Oudekerkerdijk 7, 1096 AC Amsterdam, the Netherlands
[d] Radboud University, Heyendaalsweg 135, 6525 AJ Nijmegen, the Netherlands

ARTICLE INFO

Keywords:
Internal phosphorus loading
Iron treatment
Lake restoration
Sediment geochemistry
Shallow peat lake

ABSTRACT

Internal phosphorus (P) loading is a key water quality challenge for shallow lakes. Addition of iron (Fe) salts has been used to enhance P retention in lake sediments. However, its effects on sediment geochemistry are poorly studied, albeit pivotal for remediation success. Here, we assess the factors controlling the retention of P and long-term effects following application of $FeCl_3$ (0.5–1 mol Fe/m^2, 2010) in the eutrophic, shallow peat lake Terra Nova (the Netherlands). Treatment reduced P levels in the lake for two years, but afterwards summer release of P intensified, resulting in higher surface water P concentrations than before treatment. Porewater and sediment analyses indicate that the majority of the added Fe is still undergoing redox cycling within the top 10 cm of sediment accounting for the binding of up to 70 % of sedimentary P. Sequential extractions further suggest that organic matter (OM) plays a key role in the resulting P and Fe dynamics: While reduction of P binding Fe(III) phases results in P release to porewaters, the produced Fe^{2+} remains bound to the solid phase presumably stabilized by OM. This causes P release from the sediments in excess to Fe during temporary low oxygen conditions in summer months, as confirmed by whole core flux incubation experiments. Quantitative coprecipitation of P with Fe upon reoxygenation of the water body is then impossible, leading to a gradual increase in surface water P. This first long-term study on a shallow peat lake underpins the role of OM for Fe cycling and the need to carefully consider the sediment properties and diagenetic pathways in the planning of Fe-amendments.

1. Introduction

Phosphorus (P) is the relevant macro-nutrient determining the trophic state of many freshwater lakes (Schindler et al., 2008). Human activity has tripled the external P input to naturally P-limited water bodies and soils by leaching and surface run-off of agricultural fertilizers, discharge of non or poorly treated wastewater and increased soil erosion (Bennett et al., 2001). However, even though nutrient management has significantly improved (eg. Kronvang et al., 2005) lakes have been slow to recover clear water state (Poikane et al., 2019). On EU territory alone, 50 % of the monitored lakes still do not meet the target of 'good ecological status' aimed for by the EU Water Framework Directive (European Environmental Agency, 2018). One reason is internal P loading caused by the release of P stored in the sediments. This so-called "legacy P" can become the major driver for lake eutrophication once external loading is reduced and can delay recovery for decades (Steinman and Spears, 2020). Shallow lakes are especially vulnerable for eutrophication induced by internal P loading due to their high sediment surface area to water column volume ratio and optimum conditions for primary production (regular mixing, year-round direct contact between photic zone and sediment surface) (Søndergaard et al., 2013, 2003). Consequently, shallow lakes show distinct internal loading-induced seasonality in lake water P concentrations. Because internal loading is typically particularly high during summer (Kozerski and Kleeberg, 1998; Søndergaard et al., 1999), this may alleviate P limitation, stimulate primary productivity, and thereby greatly impact ecosystems (Jeppesen et al., 2005).

One approach to reduce internal P loading is to use iron (Fe) to increase the retention of P in the sediment. This is based on the ability of Fe to sequester P by co-precipitation and adsorption (Gunnars et al.,

* Corresponding author.
E-mail address: m.a.munch@uu.nl (M.A. Münch).

https://doi.org/10.1016/j.watres.2023.120844
Received 26 July 2023; Received in revised form 9 October 2023; Accepted 5 November 2023
Available online 8 November 2023

2002; Lijklema, 1980), and the coupling of P to the so called "ferrous wheel", the Fe redox cycling in the sediment (e.g. Einsele, 1936; Kleeberg et al., 2012; Mortimer, 1941). Fe has been added to lakes in various forms such as $FeCl_3$, $FeCl_2$, $FeSO_4$, Fe(III)-hydroxides, $FeClSO_4$ for decades (Bakker et al., 2016; Smolders et al., 2006). Kleeberg et al. (2012, 2013) showed, that, in a dimictic lake, a single Fe treatment can suppress internal P loading for 20 years, if Fe and P are released to the water column at a ratio that allows for quantitative re-coprecipitation upon oxygenation of the hypolimnion. Studies in polymictic peat lakes show positive effects on the short term but also indications for return of internal P loading (Geurts, 2010; Immers et al., 2015; Quaak et al., 1993; Van der Molen and Boers, 1994).

Generally, Fe addition was successful over the investigated period if there were only limited effects of sulfate reduction and organic matter (OM) degradation on the ferrous wheel (Bakker et al., 2016; Smolders et al., 2006). Sulfate reduction produces sulfide (H_2S) which consumes Fe^{2+} by precipitation of Fe-sulfides, sequestring Fe deeper in the sediment where H_2S is produced (Berner, 1970; Katsev et al., 2006). Fe associates with OM forming organometallic compounds that are particularly stable under anoxic conditions (Lalonde et al., 2012) and can have a major impact on P retention (Gerke, 1993). However, Rothe et al. (2014) showed that Fe addition can enhance P burial by formation

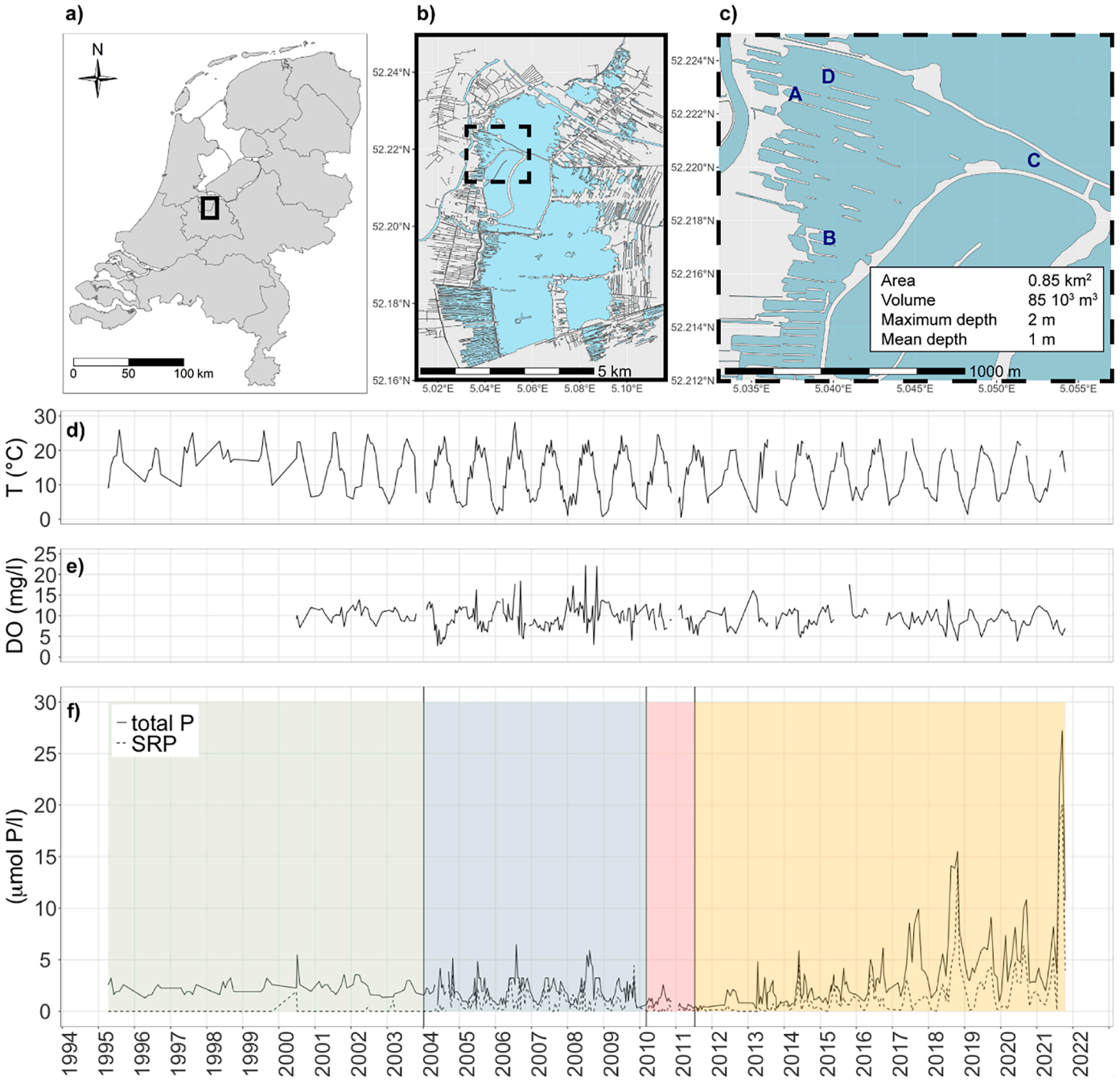

Fig. 1. The Netherlands (a) with position of the Loosdrechtse Plassen lake system (solid rectangle, b) and lake Terra Nova (dashed rectangle, c) with sampling locations for sediment cores (A, B, C) and surface water (C and D). Surface water quality monitoring data of the period 1995–2021 (courtesy of Waternet): temperature (d), dissolved oxygen (DO) concentration (e), both systematically measured at 30 cm depth, total dissolved P and SRP (f). Before 2003 no measures were taken to reduce internal loading (f, green), then burrowing fish were removed (f, blue). The lake was treated with $FeCl_3$ for 1.5 years beginning in 2010 (f, red). Subsequently, no further measures were taken (f, yellow).

of the ferrous phosphate mineral vivianite ($Fe_3(PO_4)_2{\cdot}8H_2O$).

Hence, lake properties, particularly their sediment geochemistry, may significantly influence the success and longevity of Fe treatment. Knowledge of the long-term fate of the added Fe in the sediment and its effect on sediment biogeochemical processes is essential, albeit poorly studied. Hereby we report the first long-term study on an OM-rich system. We investigated the shallow peat lake Terra Nova 10 years after Fe amendment. Detailed chemical analysis of the sediment porewater and solid phase were linked to experimental determinations of benthic fluxes and long-term surface water monitoring, to elucidate the long-term effect of the added Fe on the sediment geochemistry and the water quality. We show that Fe amendment introduced a highly redox active OM-bound Fe-pool, which accumulates P and releases it during anoxic events, which leads to seasonal peaks in internal P loading of increasing magnitude.

2. Methods

2.1. Study site

Lake Terra Nova is part of the Loosdrechtse Plassen lake system in the Netherlands formed due to peat extraction (Fig. 1a–c). Terra Nova is shallow (Fig. 1c), polymictic and characterized as eutrophic mainly due to permanent algae blooms, surface water nutrient concentrations and light climate, based on the EU Water Framework Directive (van Dijk et al., 2020). After the loss of its clear water state in the 1930s, year-round blooms of filamentous cyanobacteria prevailed from 1987 to 2004 (Fig. 1f, green period). Besides measures for external load reduction (external P load 0.11 g $P/m^2/y$ in 2010, ter Heerdt, 2012, Voort, 2019), two attempts were made to reduce internal P loading (net internal P load 0.1 g $P/m^2/y$ in 2010, ter Heerdt, 2012): removal of bream (2003, 2004, Fig. 1f, blue period) and Fe addition (2010–2011, Fig. 1f, red period, Supplementary information A) The water table of Terra Nova is maintained at constant level with maximum fluctuation of 0.1 m. This implies that hydraulic gradients between the lake and groundwater remain shallow and constrain external P load via groundwater. The main water source is precipitation and surface water from neighboring lake Loenderveen during dry periods and the main water outlet is the river Vecht (SI A).

Starting in 2010, 40 % $FeCl_3$ solution was continuously applied in low doses over a period of 1.5 years. Sediment traps installed above the sediment surface recorded a total average addition of 0.5 mol Fe/m^2 (ter Heerdt, 2012, personal communication G. ter Heerdt). The bay at station B (Fig. 1c) had been used as a test location before whole lake treatment and, consequently, received a total dose of 1 mol Fe/m^2 (ter Heerdt, 2012). For 1.5 years after Fe treatment, surface water total P and phosphate concentrations dropped below 0.5 and 0.2 μmol P/l respectively. Thereafter, concentrations increased again (Immers et al., 2015). Since 2016 the surface water total P and phosphate concentrations have been reaching higher levels than before treatment with peaks of increasing intensity in the summer months which led to renewed cyanobacterial blooms (Voort, 2019). In summer 2021, total P and phosphate reached the highest concentrations since the start of measurements at values of 27 and 20 μmol/l, respectively (Fig. 1f). For long-term data of other nutrients, see SI B.

It is unclear why the Fe addition suppressed internal P loading for only 1.5 years followed by the highest surface water P concentrations since beginning of monitoring in 1986. In this study we test the following hypothesis, conceptually based on disruption of the "ferrous wheel" (Kleeberg et al., 2012): The added Fe increased the amount of P bound in the surface sediment. Burial of the added Fe, chemically in FeS_x–phases and physically linked to high sedimentation rates, leads to increasing release of the accumulated P during summer months.

2.2. Sampling of surface water and sediment

The water column was sampled on June 22nd 2020 at two stations, C and D (Fig. 1c; SI C).

Undisturbed sediment cores (length 60 cm, ∅ 6 cm) were collected using a gravity corer (UWITEC, Mondsee, Austria) on June 22nd and July 3rd 2020 from stations A, B and C (0.4 m, 0.6 m and 1.9 m water depth, respectively) (Fig. 1c), preserving at least 10 cm of overlying water. These stations were selected as representative for the two main sedimentation regimes of the lake and the bay which received double the Fe dose (station B) (SI D).

The sediment cores were stored in a climate chamber at bottom water temperature (15 °C) and the overlying water was purged with air until further use to preserve sediment redox conditions. Within three days one core per station was sliced and processed in an N_2 glove box. Sampling resolution was 1 cm for the top 10 cm and 2 cm for the remaining core. Sediment solid phase and porewater were separated by centrifugation (10 minutes, 3000 rpm). The porewater was filtered (0.2 μm pore size nylon membrane syringe filter) and subsampled in the glovebox (SI E). The solid phase was freeze-dried assuring ventilation with N_2. Dried solid phase was homogenized in the glovebox using an agate mortar and pestle and stored at room temperature under N_2 atmosphere until further analysis.

2.3. Sediment incubation experiments

2.3.1. Experimental setup and sampling

To determine the effect of temporary bottom water anoxia on benthic fluxes of SRP (soluble reactive P) and Fe across the sediment water interface (SWI), undisturbed sediment cores from each station were incubated for 26 days at bottom water temperature (15 °C) in the dark. Per station, separate cores were incubated under oxic and anoxic conditions (SI F). The supernatant water was sampled twice a day for the first week and then every two days. Water volume extracted by sampling (10 ml) was replenished with lake water. The water samples were filtered (0.2 μm, nylon), acidified with 1 ml of 3.75 M HNO_3 and analyzed for P (oxic and anoxic) and Fe (anoxic only).

2.3.2. Calculation of benthic fluxes

Benthic flux rates were calculated by linear regression of the initial linear increase in surface water concentrations with time in the incubation experiments accounting for the surface area using the ratio of supernatant water volume to core sediment surface area (Steinman and Spears, 2020). Benthic flux rates were extrapolated to the whole lake using weighted averages of data from the three stations. Station B is representative for two bays which contribute approximately 0.8 % to the lake surface. Station A and C were assumed to contribute equally to the remaining 99.2 % of surface area as they are representative for the east of the lake with a high sedimentation regime and the west of the lake with a low sedimentation regime, respectively. In an alternative approach, in situ benthic P fluxes for the summer of 2021 were estimated based on the increase in total P in surface waters between July 21st and September 15th 2021 (Fig. 1f), and the surface area and volume of the lake.

2.4. Chemical analyses

2.4.1. Water samples

All water samples were analyzed colorimetrically for dissolved Fe species, P and H_2S using a UVmini-1240 UV–vis spectrometer of Shimadzu and disposable plastic cuvettes. Analysis for H_2S was done within a week using the methylene blue method (Lawrence et al., 2000). Total Fe and Fe^{2+} concentrations were determined using the ferrozine method (Viollier et al., 2000). Dissolved ortho-PO_4^{3-} (SRP) concentrations were obtained using the molybdenum blue method (Murphy and Riley, 1962).

2.4.2. Solid phase analysis

2.4.2.1. Total elemental contents. For the determination of total elemental composition of the freeze dried and ground sediment, between 80 and 125 mg was digested using $HClO_4$, HNO_3, and HF as described in van Helmond et al. (2018). To quantitatively digest the organic matter, an additional step was performed before overnight residual dissolution: 2.5 ml concentrated H_2O_2 and 2.5 ml concentrated HCl were slowly added and reacted until gas production stopped, followed by evaporation at 140 °C (in-house method). Digests were analyzed by ICP-OES. Average analytical uncertainty based on duplicates ($n = 10$), in-house standards and reference material (ISE-921) was 3 % for P, 3 % for Fe, 2 % for Al and 3 % for S.

Total organic carbon (TOC) of the sediment solid phase was determined according to van Helmond et al. (2018) using a Fisons Instruments NA 1500 NCS analyzer and nicotinamide as a standard (certified content 59.01 wt% TOC). The average measured value for nicotinamide ($n = 9$) was 59.3 ± 0.8 wt% TOC. Average analytical uncertainty based on duplicate samples ($n = 6$) was 0.8 wt%.

2.4.2.2. P sequential extraction. P speciation of the sediment solid phase was determined using an extraction scheme based on several studies (Table 1, SI G). Samples were handled under N_2 - atmosphere up to step VI. Extracts were analyzed for P colorimetrically (Murphy and Riley, 1962) using the respective extractant as reference matrix. CDB extracts were analyzed by ICP-OES. Average analytical uncertainty based on duplicates ($n = 6$) was 26 % for P_{MgCl_2}, 8 % for P_{NaHCO_3}, 14 % for P_{CDB}, 12 % for P_{NaAc}, 7 % for P_{HCl}, and 4 % for $P_{550\ °C/HCl}$.

2.4.2.3. Fe sequential extraction. Fe speciation of the sediment solid phase was determined using an extraction scheme based on several studies (Table 2; SI H). Samples were handled under N_2 - atmosphere up to step V. CDB and HNO_3 extracts were analyzed for elemental composition using ICP-OES. The other extracts were analyzed for total Fe and Fe(II) using the ferrozine method (Stookey, 1970). Average analytical uncertainty based on duplicates ($n = 6$) was 24 % for Fe_{Asc}, 14 % for Fe_{HCl}, 45 % for Fe_{CDB}, 20 % for Fe_{Ox}, and 11 % for Fe_{HNO_3}. The sum of all extractable Fe is termed reactive Fe (Fe_{reac}), based on the reasoning from (Poulton and Canfield, 2005).

Table 1
Sequential P extraction scheme.

Steps	Extractants	Time	Target phase	Term	References
I	1 M $MgCl_2$ (pH 8)	0.5 h	Exchangeable P	P_{MgCl_2}	(Slomp et al., 1996)
II_a	1 M $NaHCO_3$ (pH 7.6)	16 h	OM-associated P	P_{NaHCO_3}	based on (Baldwin, 1996)
II_b	1 M $MgCl_2$ (pH 8)	0.5 h	Washing step		(Parsons et al., 2017)
III_a	CDB solution (pH 7.6): 0.3 M Na_3 citrate, 25 g/L Na dithionite, 1 M $NaHCO_3$	8 h	P bound to Fe oxides	P_{CDB}	(Slomp et al., 1996)
			Fe(II)-phosphates[a] CaCO3 – P[b]		
III_b	1 M $MgCl_2$ (pH 8)	0.5 h	Washing step		
IV_a	1 M Na acetate buffered to pH 4 with acetic acid	6 h	Authigenic apatite	$P_{NaAc/HCl}$	
IV_b	1 M $MgCl_2$ (pH 8)	0.5 h	Washing step		
V	1 M HCl	24 h	Detrital apatite		
VI	Ashing at 550 °C 1 M HCl	2 h 24 h	Organic P	$P_{550\ °C/HCl}$	

[a] Fe(II) – phosphates (e.g. vivianite) (Dijkstra et al., 2016; Nembrini et al., 1983).
[b] P coprecipitated with $CaCO_3$ (Kraal et al., 2017).

Table 2
Sequential Fe extraction scheme.

Steps	Extractants	Time	Target phase	Term	References
I	Ascorbate solution (pH 7.5): 0.057 M ascorbic acid, 0.17 M Na_3 citrate, 0.6 MM $NaHCO_3$	24 h	Easily reducible Fe (oxyhydr) oxides	Fe_{Asc}	(Raiswell et al., 2010)
II	1 M HCl	4 h	Acid soluble Fe: Fe(II): FeS[a] Fe(III): amorphous Fe (oxyhydr) oxides	Fe_{HCl} : Fe $(II)_{HCl}$ Fe $(III)_{HCl}$	(Claff et al., 2010)
III	CDB solution (pH 4.8): 0.35 M glacial acetic acid, 0.2 M Na citrate, 50 g/L Na dithionite	4 h	Crystalline Fe (oxyhydr) oxides	Fe_{CDB}	
IV	Oxalate solution (pH 3.2): 0.2 M Ammonium oxalate, 0.17 M oxalic acid	6 h	Magnetite	Fe_{Ox}	(Lovley and Phillips, 1987; McKeague and Day, 1966)
V	Conc. HNO_3 (65–70 %)	2 h	Pyrite	Fe_{HNO_3}	(Claff et al., 2010)
–	–	–	All extractable Fe	Fe_{reac}	Based on (Poulton and Canfield, 2005)

[a] Supplementary information F.

2.4.2.4. Scanning electron microscopy. Two sediment samples from station A (5 and 38 cm depth) were assessed with scanning electron microscopy – energy dispersive X-ray spectroscopy (SEM-EDS) using a Zeiss EVO 15 SEM with two Bruker X-flash 6160 EDS detectors. Freeze-dried and homogenized samples were mounted onto a SEM stub using carbon tape under N_2 atmosphere and coated with platinum. Regions of interest were identified optically on which SEM and EDS imaging was performed.

3. Results

3.1. Surface water

At the time of sample collection in June 2020, stations A, B, C and D had a water depth of 0.2, 0.5, 1.5 and 1.6 m, respectively. The surface water was investigated at stations C and D only. Station C had 7.11 mg O_2/l in the entire water column. Station D had 2.65 mg O_2/l at the surface and 0.14 mg O_2/l in the bottom water. Electric conductivity, pH and temperature were uniform with water depth at both stations (SI C).

3.2. Sediment properties

The sediment consisted of peat with a TOC content of around 37 wt% (Fig. 2) which corresponds to an organic matter content of 63 wt% (conversion factor of 1.7 for water saturated vascular plant peat (Klingenfuß et al., 2014)). The top 10 cm were liquid and unconsolidated with a porosity of 98 %, underlaid by pasty, more consolidated layers with porosity declining to 92 % at 40 cm depth (SI I). According to the ^{210}Pb dating (Sanchez-Cabeza and Ruiz-Fernández, 2012), the year of Fe addition (2010) corresponded to ca. 13 cm sediment depth at station A and ca. 10 cm at stations B and C. The average sedimentation rate in the consolidated part of the sediment was estimated at 0.6 ± 0.1 cm/y (SI J).

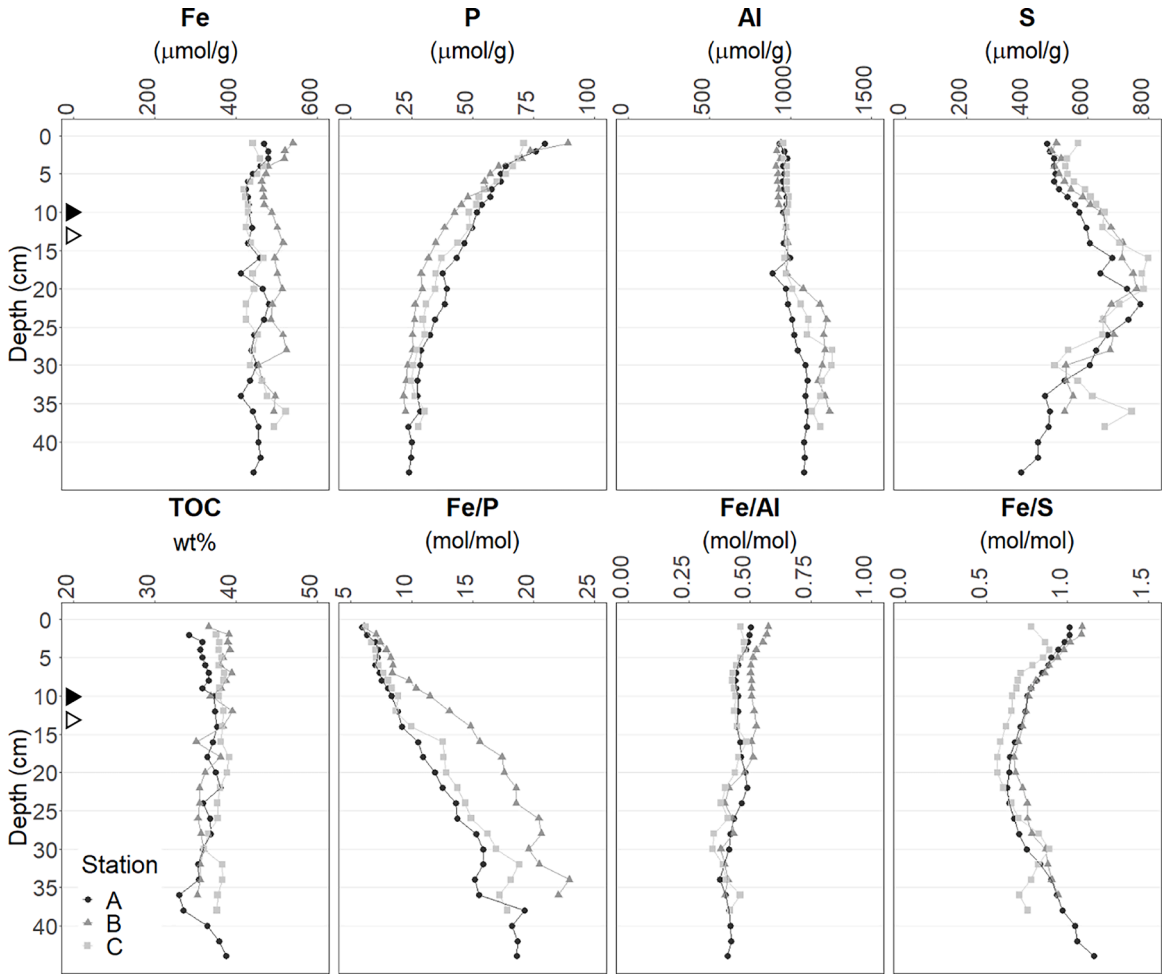

Fig. 2. Total elemental composition of the sediment solid phase. All concentrations and ratios are per g dry weight. Void (station A) and filled (stations B and C) triangles indicate the depth approximately corresponding to 2010, the year of Fe-addition (SI J).

3.3. Chemistry of the sediment solid phase

Total elemental contents did not vary significantly among stations, except for Fe. Contents varied between approximately 450–540 µmol Fe/g in the top 5 cm, while the deeper layers had lower Fe contents with no clear trend with depth (stations A, C: ca. 445 µmol Fe/g; station B: ca. 490 µmol Fe/g). At station B, total Fe contents were systematically higher compared to the other stations, with the most pronounced difference in the top 3 cm. Higher Fe contents in the top sediment coincided with higher Fe/Al ratios (Fig. 2). At all stations, $Fe(II)_{HCl}$ was the largest Fe pool in the surface sediment followed by Fe_{Asc} and Fe_{CDB}. Station B contained 50–100 % more Fe_{Asc} and Fe_{CDB} in the top 5 cm of sediment than the other stations, with Fe_{Asc} predominantly accounting for the higher total Fe content (Fig. 3a). The contribution of Fe_{Asc} to Fe_{reac} was highest at the top with a minimum around 20 cm. Fe_{HNO_3} showed the opposite pattern. The contribution of $Fe(II)_{HCl}$ to Fe_{reac} was approximately constant with depth except at Station B, where it was lower in the top 5 cm which had higher Fe_{Asc} (Fig. 3b).

Total P contents were on average 75 µmol P/g at the SWI and declined towards 25 µmol P/g. Fe/P ratios were around 6 at the SWI and increased with depth at all stations, with station B showing the most pronounced increase (Fig. 2). Organic P was the largest pool throughout the sediment with lower contributions in the top 10 cm. There, P_{CDB} and P_{NaHCO_3} each accounted for up to 30 % of total P with around 20 µmol P/g. However, at station B, P_{CDB} contributed 40 % close to the SWI, whereas P_{NaHCO_3} only contributed half as much. Below 10 cm P_{CDB} and P_{NaHCO_3} contents stayed stable at around 5 µmol P/g. There, $P_{NaAc/HCl}$ was the second largest pool, reaching 18 % contribution below 30 cm (Fig. 4). P sequential extraction yielded quantitative recovery of P within the 10 % error margin.

Sulfur was present at comparable amounts to Fe with a distinct peak around 20 cm depth at all stations. Maximum Fe_{HNO_3} coincided with maximum S contents and, correspondingly, to minimum Fe/S ratios of 0.50–0.75 mol/mol. Fe/S ratios were about 1 mol/mol at the top and bottom of the sediment. (Figs. 2 and 3). SEM analyses revealed that Fe hotspots mostly coincided with regions of elevated S content with clearly discernable framboidal (5 cm and 38 cm depth, Fig. 5a–d) and euhedral (38 cm depth, Fig. 5c and d) pyrite. Non-hotspot Fe was diffusely distributed, indicating association with the organic matrix (Fig. 5c and d).

3.4. Chemistry of the porewater

Oxygen penetration depth was 2.7, 1.2 and 2.7 mm at stations A, B and C, respectively (SI K). The porewater profiles of SRP and Fe were similar, while H_2S mirrored them: concentrations of SRP and Fe peaked around 5 cm and had a minimum around 15 cm, where H_2S concentrations peaked. At 5 cm, SRP and Fe concentrations were around 100 µmol P/l and 50 µmol Fe/l. H_2S became detectable below 1 cm, reaching ca. 60, 40 and 75 µmol S/l at 15 cm depth at stations A, B and C, respectively, and stabilizing around 7 µmol S/l below the peak (Fig. 6).

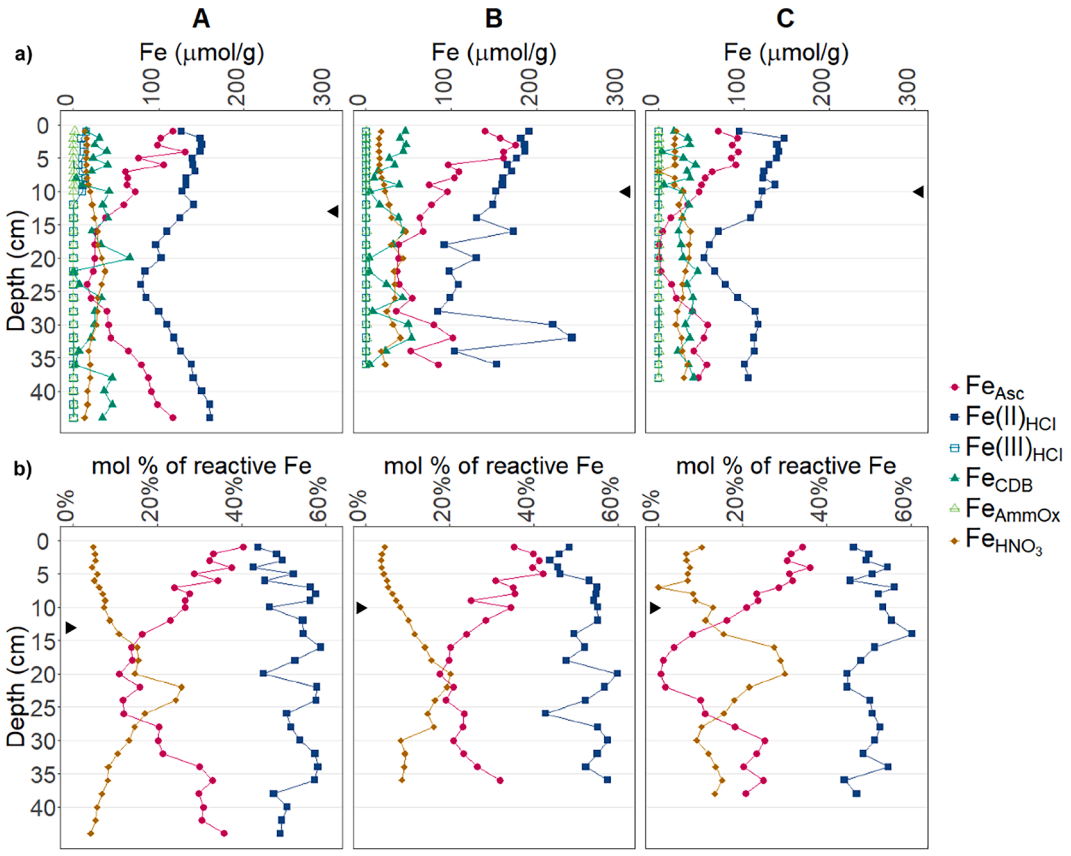

Fig. 3. Reactive sedimentary Fe pools at stations A, B, and C based on sequential Fe extraction. (a) Concentrations per sediment dry weight; (b) Contribution of the three main Fe pools to reactive Fe content in mol% including Fe_{Asc}, $Fe(II)_{HCl}$ and Fe_{HNO_3}. Black triangles indicate the depth approximately corresponding to 2010, the year of Fe-addition (SI J).

3.5. Sediment incubation experiments

Under oxic conditions, SRP concentrations in the overlying water continuously increased until the end of the experiment (Fig. 7). Oxic benthic fluxes varied largely between stations with station A having the lowest and station B the highest flux (Table 3a). Under anoxic conditions SRP concentrations in the overlying water increased over the first eight days and then plateaued at around 4 and 7 mmol P/m^2 at stations A and C, respectively. At station B they increased throughout the experiment, reaching 5 mmol P/m^2 (Fig. 7). Anoxic benthic fluxes only showed 10 % variation among stations and were lowest at station B and highest at station C (Table 3a). The corresponding whole lake weighted average P flux was around 505 µmol P m^{-2} d^{-1} (Table 3a), while the whole lake P flux estimated from the summer peak in-situ total P concentrations was approximately 420 µmol P m^{-2} d^{-1} (Table 3b).

Fe concentrations were only measured in the anoxic experiments, where they evolved similarly between stations showing a continuous increase during the first 15 days with a corresponding benthic flux of 73 ± 3 µmol Fe/m^2/d (Fig. 7, Table 3a).

The sediment released 10–84 times more P under anoxic than under oxic conditions and 5–7 times more P than Fe under anoxic conditions (Table 3).

4. Discussion

4.1. Fate of added Fe

Fe addition in 2010 increased the solid phase total Fe concentrations in the top 5 cm of sediment according to mass balance calculations (SI L). The enrichment is reflected in elevated Fe/Al ratios, which is in line with enhanced deposition of Fe-(oxyhydr)oxides formed after hydrolysis of added $FeCl_3$. Station B, which received double the Fe dose, shows the most pronounced enrichment (Fig. 2). The added Fe does not occur as a distinct peak at ca. 10 cm depth (2010, year of Fe addition: SI J), but distributed over the top 5 cm, indicating effective mobilization and reprecipitation by redox processes or sediment mixing, or both, rather than just burial.

The porewater profiles suggest that redox cycling contributes to the redistribution of added Fe. Porewater Fe^{2+} concentrations peak at 5 cm depth while Fe^{3+} is present in the top cm. Solid phase Fe(III) is thus reduced in the zone influenced by Fe-addition, releasing Fe^{2+} which is oxidized by O_2 close to the SWI. The solubility of Fe(III)-hydroxides is low in aqueous solution around neutral pH, leading to Fe^{3+}_{eq} – concentrations below 0.1 nmol/l in the absence of other complexing ligands (Stumm and Morgan, 2012). Measured porewater Fe^{3+} concentrations >10 µmol/l are indicative of Fe(III)-colloids or Fe(III) complexed by OM which are, both, able to pass the filters used for porewater sampling. This suggests that part of the reactive Fe(III) occurs associated with OM and as such undergoes redox cycling. Fe(III) is predominately recovered as Fe_{Asc}, the only Fe pool noticeably increased in the top 5 cm (Fig. 3a and b). Fe_{Asc} is redox sensitive, representing Fe(III) phases with low crystallinity such as ferrihydrite (Raiswell et al., 2010). OM can stabilize ferrihydrite, slow down sulfidation kinetics (Thomasarrigo et al., 2020) and inhibit its aging into more crystalline forms, while still allowing for electron transfer and exchange of Fe-ions with the aqueous phase (Eusterhues et al., 2008; Thomasarrigo et al., 2018; Zhou et al., 2018). OM also forms complexes with Fe^{2+} and Fe^{3+} (Sundman et al., 2014) and retains Fe in soils, particulate matter, and sediment (Lalonde et al., 2012). Thus, the added Fe likely increased the OM-associated Fe pool, consisting of a mixture of ferrihydrite and complexed Fe. Consequently, Fe^{2+} produced by reduction of this Fe pool may partially stay bound to OM instead of being released into the porewater.

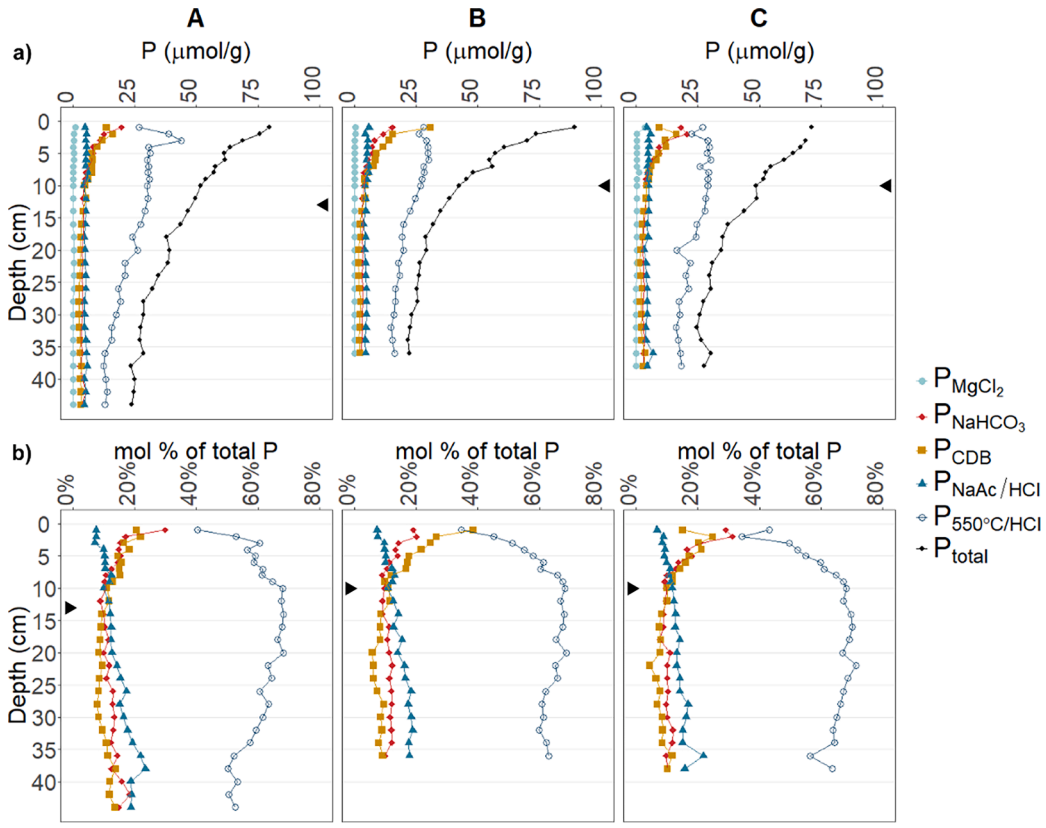

Fig. 4. Extractable P pools at stations A, B, and C based on sequential P extraction. (a) Concentrations per sediment dry weight; (b) Relative contribution of each pool to total P content. Black triangles indicate the depth approximately corresponding to 2010, the year of Fe-addition (SI J).

However, diffusive transport of Fe to the sediment surface is insufficient to compensate for the burial of solid-bound Fe. The average Fe^{2+} diffusive flux in the top 5 cm is 7.1 ± 0.6 nmol m^{-2} y^{-1} (SI M), while the average total Fe burial flux, 0.14 ± 0.03 mol m^{-2} y^{-1} (SI J), is eight orders of magnitude larger. This implies that mixing of the top sediment is the main driver for Fe redox cycling, exposing both dissolved Fe^{2+} and solid-bound Fe(II) to oxidizing conditions. In Terra Nova the top sediment is highly unconsolidated and thus prone to resuspension, as was also reported for other shallow lakes (Jalil et al., 2019). The ^{210}Pb profiles suggest occasional mixing of the top 10 cm, as unsupported ^{210}Pb contents show no consistent trend. Below 10 cm, they decrease exponentially as expected for constant burial rates in the absence of mixing (SI J).

Sporadic mixing also explains the presence of FeS and FeS_2 in the top sediment, although concomitant O_2 supply limits the sulfidation of Fe (III)-phases. Lasting sulfidation and thus burial of Fe is restricted to the sediment below 10 cm depth. There, increase in solid phase Fe_{HNO_3} at the expense of Fe_{Asc} (Fig. 3), porewater H_2S maxima (Fig. 6) and abundant euhedral pyrite (Fig. 5c,d) indicate pyrite formation (Fig. 6). The Fe burial flux between 10 and 20 cm depth is 10 ± 2 mmol Fe m^{-2} y^{-1} (SI J), implying complete burial of the single Fe dose of 500 mmol Fe/m^2 within 50 years. FeS on the other hand is probably also formed in the top 10 cm below the oxygen penetration depth. However, this process was not enhanced by Fe-addition as $Fe(II)_{HCl}$ does not show increased contents in that layer (Fig. 3b). This all implies that, so far, sulfidation has not been an important sink for the added Fe.

4.2. Effect of added Fe on P dynamics

Fe addition enhanced binding of P by reactive Fe phases as indicated by increased contents of P_{CDB} and P_{NaHCO_3} in the top 10 cm of sediment, where they contribute 40 % and 30 % to solid phase total P, respectively (Fig. 4b). P_{CDB} corresponds to P bound to Fe (oxyhydr)oxides, while P_{NaHCO_3} corresponds to P associated to OM (Table 1). Association of P to OM can occur in the form of ternary complexes with Fe, Al, or Ca as bridging ions (Gerke, 2010; Guardado et al., 2007), or as P bound to colloidal Fe(III) (oxyhydr)oxides stabilized by OM (Dolfing et al., 1999). Hence, up to 70 % of sedimentary P is bound to Fe in the zone influenced by Fe addition. About half of this P is bound to Fe which is associated to OM. Below 10 cm depth, Ca-bound P is the dominant mineral P-pool ($P_{NaAc/HCl}$, Table 1, Fig. 4b) indicating that before Fe-addition apatite formation or co-precipitation of P with calcite had quantitatively more impact on the sediment P dynamics than Fe redox cycling. Further, $P_{NaAc/HCl}$ concentrations are stable with depth (Fig. 4a), implying that Ca—P mineral formation has been occurring unchanged since Fe treatment, but 10 years might still be insufficient to reflect changes on long-term P burial. Fe-addition thus changed the P dynamics of the system predominately by introducing an additional, redox-sensitive sink for P to the surface sediment.

Fe reduction is therefore expected to be the main cause for P mobilization in the surface sediment, which is supported by the correlating P and Fe porewater profiles (Fig. 6, SI K). The sediment incubation experiments further support redox dependent release of P to the surface water as P fluxes were two orders of magnitude higher under anoxic than under oxic conditions (Table 3). However, seven times more P than Fe was released during anoxic incubation (Table 3) and porewater P/Fe ratios range between 1.3 and 4.3 mol/mol in the top 10 cm. These ratios exceed the P/Fe ratio in the solid phase pools that represent P—Fe association by one order of magnitude ($[P_{NaHCO_3} + P_{CDB}] / [Fe_{Asc} + Fe(III)_{HCl} + Fe_{CDB}] = P_{P\text{-}Fe} / Fe_{P\text{-}Fe} < 0.4$ mol/mol) (Fig. 8). As discussed in Section 4.1, OM can stabilize Fe^{2+} in the solid phase which, in such an OM-rich system, may be the main reason for the excessive P release with respect to the solid phase P/Fe ratio. This dynamic represents a disruption of the "ferrous wheel", as not enough Fe^{2+} will be present in

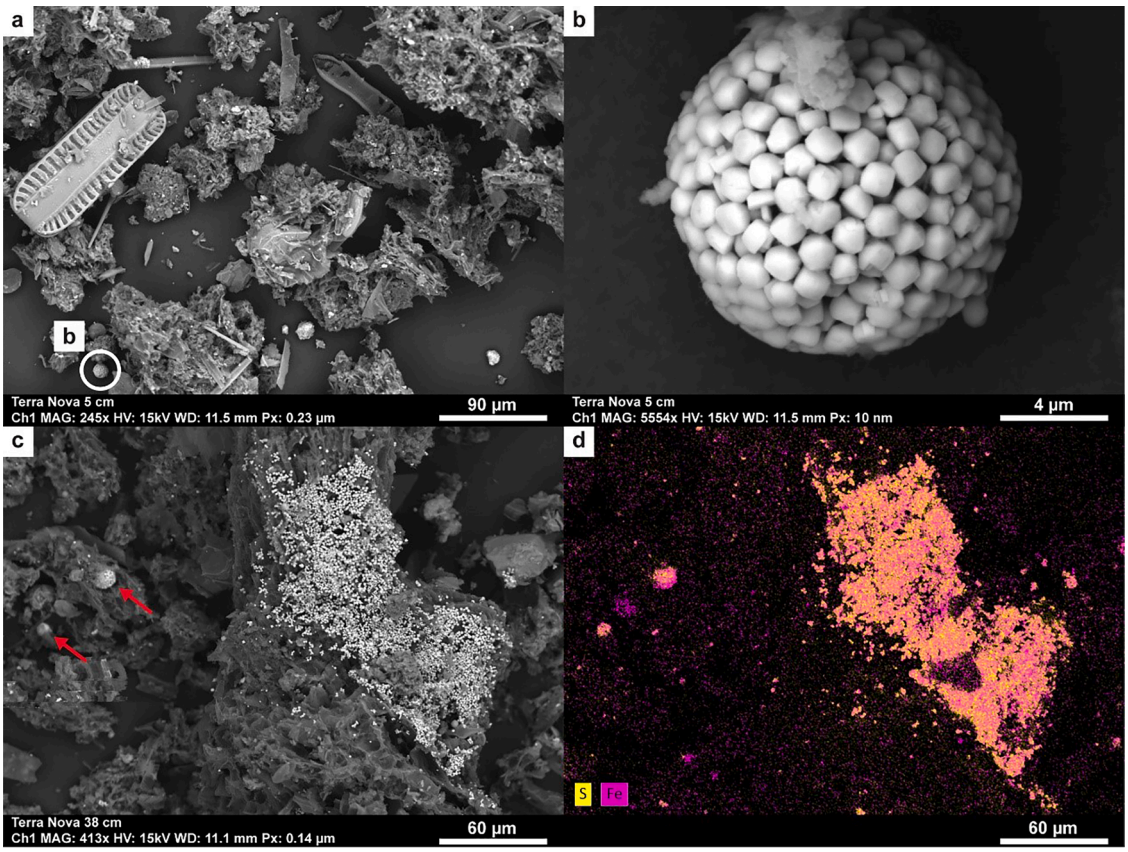

Fig. 5. SEM images of sediment samples from Station A. At 5 cm depth (a and b) a pyrite framboid is visible as indicated by the circle in (a) and at higher magnification in (b). The sample at 38 cm depth (c and d) shows diffuse distribution of Fe with regions of high abundance of Fe coinciding with high abundance of S according to EDS mapping (d). Especially recognizable is a large accumulation of euhedral pyrite crystals and two pyrite framboids. The latter are indicated by arrows (c).

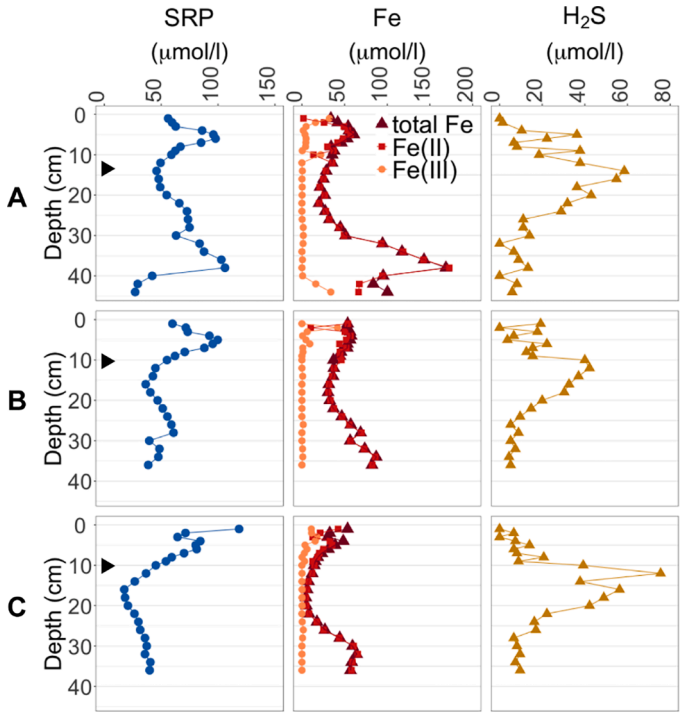

Fig. 6. Porewater concentrations of SRP, Fe (including speciation) and sulfide (H_2S) for stations A, B and C, respectively. Black triangles indicate the depth approximately corresponding to 2010, the year of Fe-addition (SI J).

the water body for quantitative coprecipitation of P and Fe, once oxidizing conditions return after temporary bottom water anoxia.

The solid phase The $P_{P\text{-}Fe}/Fe_{P\text{-}Fe}$ ratios found in the surface sediment exceed 0.12 mol/mol (Fig. 8b), indicating that adsorption capacity of Fe for P is insufficient to reimmobilize the P released by Fe reduction. The threshold of 0.12 mol/mol was found empirically for systems with P mobilization due to Fe reduction, as at higher P/Fe ratios insufficient sorption sites are available to adsorb the released P (Hilbrandt et al., 2019; Smolders et al., 2017; Xia, 2022). P mobilized by Fe reduction in the surface sediment due to bottom water anoxia would thus be expected to reach the surface water. Surface water measurements suggest the occurrence of local anoxic spells in shallow lake Terra Nova during the summer months (SI C). Mass balance calculations confirm that periodic bottom water anoxia can account for the summer peaks in surface water P concentrations: benthic P fluxes measured in the incubation experiments under anoxic conditions and extrapolated to the whole lake (505 $\pm$ 51 µmol/$m^{2/}$d) exceed the required P flux needed for the peak in surface water total P concentrations in 2021 (420 µmol/m^2/d) (Table 3). These fluxes are the highest since beginning of monitoring and comparable to what is reported in the literature for shallow polymictic lakes (SI B). Further, the inventory of reactive P in the sediment layer above the oxygen penetration depth (SI K), the layer susceptible to temporary bottom water anoxia, is large enough to account for summer peak P concentrations.

The increasing amplitude of the seasonal surface water P peaks (Fig. 1f) indicates an increase in the redox-sensitive P-pool in the surface sediment over time. Indeed, the solid phase $P_{P\text{-}Fe}$ / $Fe_{P\text{-}Fe}$ ratios of < 0.4 mol/mol (Fig. 8b) suggest that capacity of the redox-active Fe in the top sediment to bind P by co-precipitation is not exhausted. (van der Grift et al., 2016) found P/Fe ratios of maximum 0.6 mol/mol in P—Fe

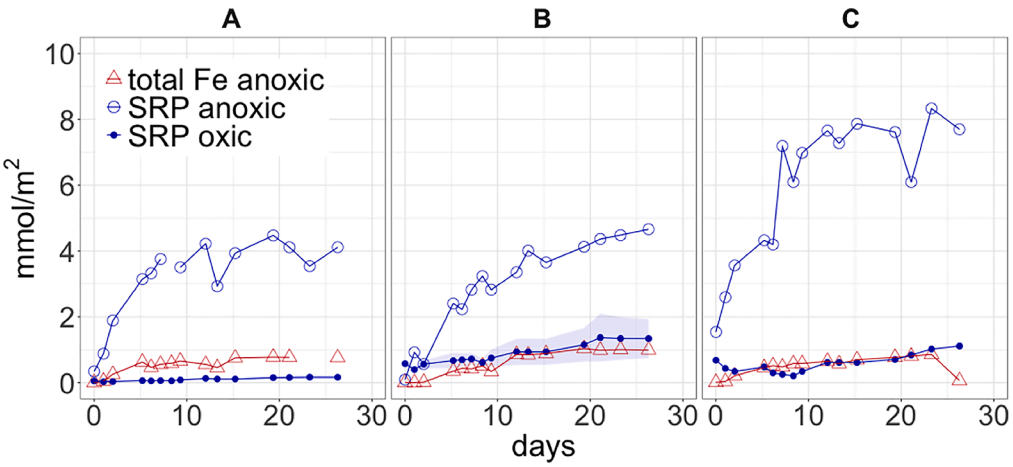

Fig. 7. Evolution of the concentration of SRP (circles) and total Fe (triangles) in the supernatant water of the oxic (filled) and anoxic (open) incubation experiments at stations A, B and C.

Table 3
Benthic fluxes for the individual stations and extrapolated to the whole lake as measured in the incubation experiments (a) and estimated from in situ total P concentrations measured in the surface water monitoring (b). Ratios are the ratios of the fluxes. Whole lake averages calculated from the incubation experiments are weighted for their contribution to sediment surface area.

	Oxic **P** ($\mu mol/m^2/d$)	Anoxic **P** ($\mu mol/m^2/d$)	Anoxic/Oxic **P**	Anoxic **Fe** ($\mu mol/m^2/d$)	Anoxic **P/Fe**
a)					
Station A	5.54	466	84	70.4	6.6
Station B	36.1	365	21	69.9	5.2
Station C	25.8	546	10	75.6	7.2
Whole lake average	16 ± 13	505 ± 51	52 ± 39	73 ± 3	6.9 ± 0.4
b)					
In situ P flux (15.9 – 21.7.2021)	420 $\mu mol\ P/m^2/d$				

co-precipitates formed upon oxidation of Fe^{2+} in natural waters. When also Ca^{2+} is present, P/Fe ratios of 1 mol/mol can be reached for conditions comparable to the porewater compositions encountered in the top sediments of Terra Nova (Senn et al., 2015). However, aging of the precipitates leading to more crystalline Fe solids can be accompanied by a decrease in P/Fe ratios (Senn et al., 2017), but the aging can be delayed in the presence of dissolved phosphate at solution P/Fe ratios exceeding 0.55 (Voegelin et al., 2013). Gerke and Hermann (1992) reported the sorption maximum of P to Al and Fe complexed by organic matter to exceed 0.5 mol P/mol (Fe+Al), while theoretically, ternary complexes of P, Fe and OM could reach a P/Fe-stoichiometry of 1. The redox-active Fe-bound P pool in the surface sediment can thus still be expected to increase, which potentially leads to even higher summer surface water P concentrations.

The data collected in this study suggests that the Fe-addition introduced a significant reactive Fe-pool to the surface sediment. Due to recurring mixing of the surface sediment and association to OM, the added Fe still undergoes redox cycling in the top 10 cm of sediment and was not quantitatively buried in sulfide phases. This Fe pool represents a highly redox active sink for P, enriching it over the years, while not providing enough sorption capacity to bind the P released by Fe reduction. Additionally, Fe^{2+} is stabilized in the solid phase by OM, causing P release to exceed Fe release with respect to solid phase P/Fe. This situation has been amplifying the linkage between Fe reduction and P release during events of bottom water anoxia, which is reflected in the increasing trend in lake water total P and ortho-phosphate concentrations since Fe treatment (SI N). Furthermore, the top sediment still has the capacity to enrich the reactive Fe-bound P pool by co-precipitation upon reoxidation of reductively released Fe, which will likely result in

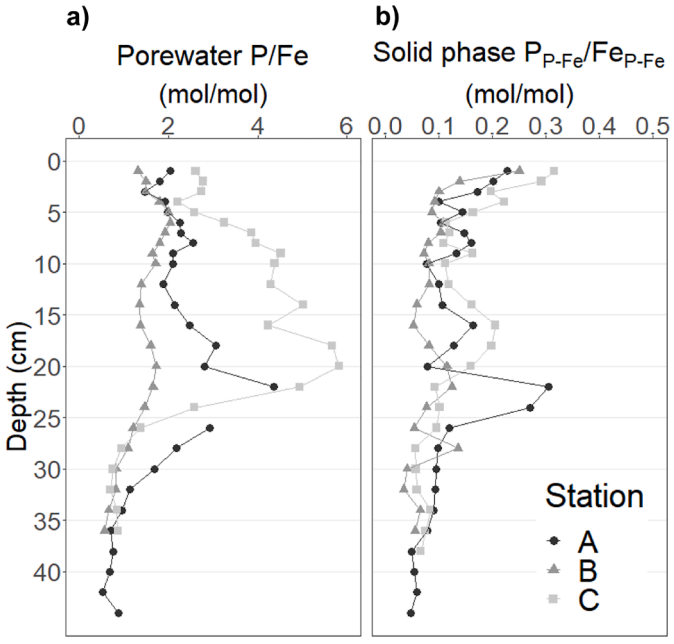

Fig. 8. Molar P/Fe ratios in (a) the porewater and (b) the solid phase. Solid phase $P_{P\text{-}Fe}/Fe_{P\text{-}Fe} = [P_{NaHCO_3} + P_{CDB}]/[Fe_{Asc} + Fe(III)_{HCl} + Fe_{CDB}]$ corresponds to the ratio of solid phase P associated to Fe and solid phase Fe with affinity to P based on the sequential extractions of P (Table 1) and Fe (Table 2).

further intensification of seasonal internal P loading in Terra Nova.

5. Conclusion

This study suggests that $FeCl_3$ is not suitable to remediate internal P loading in dynamic lake systems such as Terra Nova that are high in OM and undergo frequent sediment mixing and changes in oxygen availability. The introduction of a highly reactive Fe source to such systems favors the formation and enrichment of a highly redox sensitive P pool, leading to the intensification of seasonal internal P loading. It remains to be investigated whether the addition of Fe in a less reactive form (e.g. Fe (oxyhydr)oxides) would be a better alternative, as it would probably allow for higher dosing and be less prone to form associations with OM.

Declaration of Competing Interest

The authors declare that they have no known competing financial interests or personal relationships that could have appeared to influence the work reported in this paper.

Data availability

Data will be made available on request.

Acknowledgments

This research was part of the P-Trap project funded by the European Union's Horizon 2020 research and innovation program under the Marie Skłodowska-Curie grant agreement No 813438. We acknowledge the Utrecht University laboratory staff H.C. de Waard, J.M. van Aken, J.J. Mulder, J.J. van Tongeren, J.G.J. Visser, J.P. de Witte, M. Hamers and T. H.H. Claessen for chemical analysis, the fabrication of lab-ware, and general support, A. Cinjee from Deltares for help with field equipment and sampling and Dr. N.A.G.M. van Helmond and Dr. M. Hermans for consultation and help with laboratory work. We further thank Dr. Gertrud Nürnberg and an anonymous reviewer for their constructive feedback.

Supplementary materials

Supplementary material associated with this article can be found, in the online version, at doi:10.1016/j.watres.2023.120844.

References

Bakker, E.S., Van Donk, E., Immers, A.K., 2016. Lake restoration by in-lake iron addition: a synopsis of iron impact on aquatic organisms and shallow lake ecosystems. Aquat. Ecol. 50, 121–135. https://doi.org/10.1007/s10452-015-9552-1.

Baldwin, D.S., 1996. The phosphorus composition of a diverse series of Australian sediments. Hydrobiologia 335, 63–73. https://doi.org/10.1007/BF00013684.

Bennett, E.M., Carpenter, S.R., Caraco, N.F., 2001. Human impact on erodable phosphorus and eutrophication: a global perspective: increasing accumulation of phosphorus in soil threatens rivers, lakes, and coastal oceans with eutrophication. Bioscience 51, 227–234.

Berner, R.A., 1970. Sedimentary pyrite formation. Am. J. Sci. 268, 1–23.

Claff, S.R., Sullivan, L.A., Burton, E.D., Bush, R.T., 2010. A sequential extraction procedure for acid sulfate soils: partitioning of iron. Geoderma 155, 224–230. https://doi.org/10.1016/j.geoderma.2009.12.002.

Dijkstra, N., Slomp, C.P., Behrends, T., 2016. Vivianite is a key sink for phosphorus in sediments of the Landsort Deep, an intermittently anoxic deep basin in the Baltic Sea. Chem. Geol. 438, 58–72. https://doi.org/10.1016/j.chemgeo.2016.05.025.

Dolfing, J., Chardon, W., Japenga, J., 1999. Assiciation between colloidal iron, aluminum, phosphorus and humic acids. Soil Sci. 164, 171–179.

Einsele, W., 1936. Über die Beziehungen des Eisenkreislaufs zum Phosphatkreislauf im eutrophen See. Arch. Hydrobiol. 29, 664–686.

European Environmental Agency, Zal, N., Whalley, C., Christiansen, T., Kristensen, P., Néry, F., 2018. European waters : Assessment of Status and Pressures 2018. https://doi.org/10.2800/303664.

Eusterhues, K., Wagner, F.E., Häusler, W., Hanzlik, M., Knicker, H., Totsche, K.U., Kögel-Knabner, I., Schwertmann, U., 2008. Characterization of ferrihydrite-soil organic matter coprecipitates by X-ray diffraction and Mossbauer spectroscopy. Environ. Sci. Technol. 42, 7891–7897.

Gerke, J., Hermann, R., 1992. Adsorption of orthophosphate to humic-Fe-complexes and to amorphous Fe-oxide. Z. Pflanzenernähr. Bodenkd. 155, 233–236.

Gerke, J., 1993. Phosphate adsorption by humic/Fe-oxide mixtures aged at pH 4 and 7 and by poorly ordered Fe-oxide. Geoderma 59, 279–288. https://doi.org/10.1016/0016-7061(93)90074-U.

Gerke, J., 2010. Humic (organic matter)-Al(Fe)-phosphate complexes: an underestimated phosphate form in soils and source of plant-available phosphate. Soil Sci. 175, 417–425. https://doi.org/10.1097/SS.0b013e3181f1b4dd.

Geurts, J.J.M., 2010. Restoration of Fens and Peat lakes: a Biogeochemical Approach (Doctoral Thesis). Radboud University, Nijmegen.

Guardado, I., Urrutia, O., Garcia-Mina, J.M., 2007. Size distribution, complexing capacity , and stability of phosphate − metal − humic complexes. J. Agric. Food Chem. 55, 408–413. https://doi.org/10.1021/jf062894y.

Gunnars, A., Blomqvist, S., Johansson, P., Andersson, C., 2002. Formation of Fe(III) oxyhydroxide colloids in freshwater and brackish seawater, with incorporation of phosphate and calcium. Geochim. Cosmochim. Acta 66, 745–758. https://doi.org/10.1016/S0016-7037(01)00818-3.

Hilbrandt, I., Lehmann, V., Zietzschmann, F., Ruhl, A.S., Jekel, M., 2019. Quantification and isotherm modelling of competitive phosphate and silicate adsorption onto micro-sized granular ferric hydroxide. RSC Adv. 9, 23642–23651. https://doi.org/10.1039/C9RA04865K.

Immers, A.K., Bakker, E.S., Van Donk, E., Ter Heerdt, G.N.J., Geurts, J.J.M., Declerck, S. A.J., 2015. Fighting internal phosphorus loading: an evaluation of the large scale application of gradual Fe-addition to a shallow peat lake. Ecol. Eng. 83, 78–89.

Jalil, A., Li, Y., Zhang, K., Gao, X., Wang, W., Khan, H.O.S., Pan, B., Ali, S., Acharya, K., 2019. Wind-induced hydrodynamic changes impact on sediment resuspension for large, shallow Lake Taihu, China. Int. J. Sediment Res. 34, 205–215. https://doi.org/10.1016/j.ijsrc.2018.11.003.

Jeppesen, E., Søndergaard, M., Jensen, J.P., Havens, K.E., Anneville, O., Carvalho, L., Coveney, M.F., Deneke, R., Dokulil, M.T., Foy, B.O.B., Gerdeaux, D., Hampton, S.E., Lammens, E.H.H.R., Torben, L., 2005. Lake responses to reduced nutrient loading – an analysis of contemporary long-term data from 35 case studies. Freshw. Biol. 50, 1747–1771. https://doi.org/10.1111/j.1365-2427.2005.01415.x.

Katsev, S., Tsandev, I., L'Heureux, I., Rancourt, D.G., 2006. Factors controlling long-term phosphorus efflux from lake sediments: exploratory reactive-transport modeling. Chem. Geol. 234, 127–147.

Kleeberg, A., Köhler, A., Hupfer, M., 2012. How effectively does a single or continuous iron supply affect the phosphorus budget of aerated lakes? J. Soils Sediments 12, 1593–1603. https://doi.org/10.1007/s11368-012-0590-1.

Kleeberg, A., Herzog, C., Hupfer, M., 2013. Redox sensitivity of iron in phosphorus binding does not impede lake restoration. Water Res. 47, 1491–1502. https://doi.org/10.1016/j.watres.2012.12.014.

Klingenfuß, C., Roßkopf, N., Walter, J., Heller, C., Zeitz, J., 2014. Soil organic matter to soil organic carbon ratios of peatland soil substrates. Geoderma 410–417. https://doi.org/10.1016/j.geoderma.2014.07.010, 235–236.

Kozerski, H., Kleeberg, A., 1998. The sediments and benthic-pelagic exchange in the shallow lake müggelsee (berlin, germany). Int. Rev. Hydrobiol. 83, 77–112.

Kraal, P., Dijkstra, N., Behrends, T., Slomp, C.P., 2017. Phosphorus burial in sediments of the sulfidic deep Black Sea: key roles for adsorption by calcium carbonate and apatite authigenesis. Geochim. Cosmochim. Acta 204, 140–158. https://doi.org/10.1016/j.gca.2017.01.042.

Kronvang, B., Jeppesen, E., Conley, D.J., Søndergaard, M., Larsen, S.E., Ovesen, N.B., Carstensen, J., 2005. Nutrient pressures and ecological responses to nutrient loading reductions in Danish streams, lakes and coastal waters. J. Hydrol. 304, 274–288. https://doi.org/10.1016/j.jhydrol.2004.07.035.

Lalonde, K., Mucci, A., Ouellet, A., Gélinas, Y., 2012. Preservation of organic matter in sediments promoted by iron. Nature 483, 198–200. https://doi.org/10.1038/nature10855.

Lawrence, N.S., Davis, J., Compton, R.G., 2000. Analytical strategies for the detection of sulfide: a review. Talanta 52, 771–784.

Lijklema, L., 1980. Interaction of orthophosphate with iron (III) and aluminum hydroxides. Environ. Sci. Technol. 14, 537–541.

Lovley, D.R., Phillips, E.J.P., 1987. Rapid assay for microbially reducible ferric iron in aquatic sediments. Appl. Environ. Microbiol. 53, 1536–1540. https://doi.org/10.1128/aem.53.7.1536-1540.1987.

McKeague, J.A., Day, J.H., 1966. Dithionite- and oxalate-extractable Fe and Al as aids in differentiating various classes of soils. Can. J. Soil Sci. 46, 13–22. https://doi.org/10.4141/cjss66-003.

Mortimer, C.H., 1941. The exchange of dissolved substances between mud and water in lakes. Br. Ecol. Soc. 29, 280–329.

Murphy, J., Riley, J., 1962. Colorimetric method for determination of P in soil solution. Anal. Chim. Acta 27, 31–36.

Nembrini, G.P., Capobianco, J.A., Viel, M., Williams, A.F., 1983. A Mössbauer and chemical study of the formation of vivianite in sediments of Lago Maggiore (Italy). Geochim. Cosmochim. Acta 47, 1459–1464. https://doi.org/10.1016/0016-7037(83)90304-6.

Parsons, C.T., Rezanezhad, F., O'Connell, D.W., van Cappellen, P., 2017. Sediment phosphorus speciation and mobility under dynamic redox conditions. Biogeosciences 14, 3585–3602. https://doi.org/10.5194/bg-14-3585-2017.

Poikane, S., Phillips, G., Birk, S., Free, G., Kelly, M.G., Willby, N.J., 2019. Deriving nutrient criteria to support 'good' ecological status in European lakes: an empirically based approach to linking ecology and management. Sci. Total Environ. 650, 2074–2084. https://doi.org/10.1016/j.scitotenv.2018.09.350.

Poulton, S.W., Canfield, D.E., 2005. Development of a sequential extraction procedure for iron: implications for iron partitioning in continentally derived particulates. Chem. Geol. 214, 209–221. https://doi.org/10.1016/j.chemgeo.2004.09.003.
Quaak, M., van der Does, J., Boers, P., van der Vlugt, J., 1993. A new technique to reduce internal phosphorus loading by in-lake phosphate fixation in shallow lakes. Hydrobiologia 253, 337–344. https://doi.org/10.1007/BF00050759.
Raiswell, R., Vu, H.P., Brinza, L., Benning, L.G., 2010. The determination of labile Fe in ferrihydrite by ascorbic acid extraction : methodology , dissolution kinetics and loss of solubility with age and de-watering. Chem. Geol. 278, 70–79. https://doi.org/10.1016/j.chemgeo.2010.09.002.
Rothe, M., Frederichs, T., Eder, M., Kleeberg, A., Hupfer, M., 2014. Evidence for vivianite formation and its contribution to long-term phosphorus retention in a recent lake sediment: a novel analytical approach. Biogeosciences 11, 5169–5180. https://doi.org/10.5194/bg-11-5169-2014.
Søndergaard, M., Bjerring, R., Jeppesen, E., 2013. Persistent internal phosphorus loading during summer in shallow eutrophic lakes. Hydrobiologia 710, 95–107. https://doi.org/10.1007/s10750-012-1091-3.
Søndergaard, M., Jensen, J.P., Jeppesen, E., 1999. Internal phosphorus loading in shallow danish lakes. Shallow Lakes' 98: trophic interactions in shallow freshwater and brackish waterbodies 145–152.
Søndergaard, M., Jensen, J.P., Jeppesen, E., 2003. Role of sediment and internal loading of phosphorus in shallow lakes. Hydrobiologia 506, 135–145.
Sanchez-Cabeza, J.A., Ruiz-Fernández, A.C., 2012. 210Pb sediment radiochronology: an integrated formulation and classification of dating models. Geochim. Cosmochim. Acta 82, 183–200. https://doi.org/10.1016/j.gca.2010.12.024.
Schindler, D.W., Hecky, R.E., Findlay, D.L., Stainton, M.P., Parker, B.R., Paterson, M.J., Beaty, K.G., Lyng, M., Kasian, S.E.M., 2008. Eutrophication of lakes cannot be controlled by reducing nitrogen input: results of a 37-year whole-ecosystem experiment. Proc. Natl. Acad. Sci. U.S.A. 105, 11254–11258. https://doi.org/10.1073/pnas.0805108105.
Senn, A.C., Kaegi, R., Hug, S.J., Hering, J.G., Mangold, S., Voegelin, A., 2015. Composition and structure of Fe(III)-precipitates formed by Fe(II) oxidation in water at near-neutral pH: interdependent effects of phosphate, silicate and Ca. Geochim. Cosmochim. Acta 162, 220–246. https://doi.org/10.1016/J.GCA.2015.04.032.
Senn, A.C., Kaegi, R., Hug, S.J., Hering, J.G., Mangold, S., Voegelin, A., 2017. Effect of aging on the structure and phosphate retention of Fe(III)-precipitates formed by Fe (II) oxidation in water. Geochim. Cosmochim. Acta 202, 341–360. https://doi.org/10.1016/J.GCA.2016.12.033.
Slomp, C.P., Epping, E.H.G., Helder, W., van Raaphorst, W., 1996. A key role for iron-bound phosphorus in authigenic apatite formation in North Atlantic continental platform sediments. J. Mar. Res. 54, 1179–1205. https://doi.org/10.1357/0022240963213745.
Smolders, A.J.P., Lamers, L.P.M., Lucassen, E.C.H.E.T., Van Der Velde, G., Roelofs, J.G. M., 2006. Internal eutrophication: how it works and what to do about it - A review. Chem. Ecol. 22, 93–111. https://doi.org/10.1080/02757540600579730.
Smolders, E., Baetens, E., Verbeeck, M., Nawara, S., Diels, J., Verdievel, M., Peeters, B., De Cooman, Baken, S., 2017. Internal loading and redox cycling of sediment iron explain reactive phosphorus concentrations in lowland rivers. Environ. Sci. Technol. 51 (5), 2584–2592.
Steinman, A.D., Spears, B.M., 2020. Internal Phosphorus Loading in lakes: Causes, Case studies, and Management. J. Ross Publishing.
Stookey, L.L., 1970. Ferrozine—a new spectrophotometric reagent for iron. Anal. Chem. 42, 779–781.
Stumm, W., Morgan, J.J., 2012. Aquatic Chemistry: Chemical Equilibria and Rates in Natural Waters. John Wiley & Sons.
Sundman, A., Karlsson, T., Laudon, H., Persson, P., 2014. XAS study of iron speciation in soils and waters from a boreal catchment. Chem. Geol. 364, 93–102. https://doi.org/10.1016/j.chemgeo.2013.11.023.
ter Heerdt, G., 2012. Ijzersuppletie in Laagveenplassen. STOWA, Nederlands.
Thomasarrigo, L.K., Byrne, J.M., Kappler, A., Kretzschmar, R., 2018. Impact of organic matter on iron(II)-catalyzed mineral transformations in ferrihydrite-organic matter coprecipitates. Environ. Sci. Technol. 52, 12316–12326. https://doi.org/10.1021/ACS.EST.8B03206/ASSET/IMAGES/LARGE/ES-2018-032068_0004.JPEG.
Thomasarrigo, L.K., Bouchet, S., Kaegi, R., Kretzschmar, R., 2020. Organic matter influences transformation products of ferrihydrite exposed to sulfide. Environ. Sci. Nano 7, 3405–3418. https://doi.org/10.1039/D0EN00398K.
van der Grift, B., Behrends, T., Osté, L.A., Schot, P.P., Wassen, M.J., Griffioen, J., 2016. Fe hydroxyphosphate precipitation and Fe(II) oxidation kinetics upon aeration of Fe (II) and phosphate-containing synthetic and natural solutions. Geochim. Cosmochim. Acta 186, 71–90. https://doi.org/10.1016/j.gca.2016.04.035.
van der Molen, D.T., Boers, P.C.M., 1994. Influence of internal loading on phosphorus concentration in shallow lakes before and after reduction of the external loading. Nutrient Dynamics and Biological Structure in Shallow Freshwater and Brackish Lakes. Springer, pp. 379–389.
van Dijk, J., Amesz, M., Ouboter, M., Moria, L., ter Heerdt, G., van der Wijngaart, T., 2020. Actualisatie KRW-waterlichamen AGV: Maatregelenprogramma 2022–2027. Waternet.
van Helmond, N.A.G.M., Jilbert, T., Slomp, C.P., 2018. Hypoxia in the Holocene Baltic sea: comparing modern versus past intervals using sedimentary trace metals. Chem. Geol. 493, 478–490. https://doi.org/10.1016/j.chemgeo.2018.06.028.
Viollier, E., Inglett, P.W., Hunter, K., Roychoudhury, A.N., Cappellen, P.Van, 2000. The Ferrozine method revisted. Appl. Geochem. 15, 785–790.
Voegelin, A., Senn, A.-C., Kaegi, R., Hug, S.J., Mangold, S., 2013. Dynamic Fe-precipitate formation induced by Fe (II) oxidation in aerated phosphate-containing water. Geochim. Cosmochim. Acta 117, 216–231.
Voort, S.van der, 2019. Eindrapport Maatregelanalyse Terra Nova. Waternet.
Xia, L., 2022. The application of iron-rich sorbents to mitigate phosphorus release from sediments in lowland rivers.
Zhou, Z., Latta, D.E., Noor, N., Thompson, A., Borch, T., Scherer, M.M., 2018. Fe(II)-catalyzed transformation of organic matter–ferrihydrite coprecipitates: a closer look using Fe ISotopes. Environ. Sci. Technol. 52, 11142–11150. https://doi.org/10.1021/acs.est.8b03407.